

TECHNICAL ADVANCE

Therapeutic Dose from a Pyroelectric Electron Accelerator

T. Z. Fullem, K. C. Fazel, J. A. Geuther and Y. Danon¹

Rensselaer Polytechnic Institute, Department of Mechanical, Aerospace and Nuclear Engineering, Troy, New York 12180

Fullem, T. Z., Fazel, K. C., Geuther, J. A. and Danon, Y. **Therapeutic Dose from a Pyroelectric Electron Accelerator.** *Radiat. Res.* **172**, 643–647 (2009).

Simple heating of pyroelectric crystals has been used as the basis for compact sources of X rays, electrons, ions and neutrons. We report on the evaluation of the feasibility of using a portable pyroelectric electron accelerator to deliver a therapeutic dose to tissue. Such a device could be mass produced as a handheld, battery-powered instrument. Experiments were conducted with several crystal sizes in which the crystal was heated inside a vacuum chamber and the emitted electrons were allowed to penetrate a thin beryllium window into the surrounding air. A Faraday cup was used to count the number of electrons that exited the window. The energy of these electrons was determined by measuring the energy spectrum of the X rays that resulted from the electron interactions with the Faraday cup. Based on these measurements, the dose that this source could deliver to tissue was calculated using Monte Carlo calculations. It was found that 10^{13} electrons with a peak energy of the order of 100 keV were emitted from the beryllium window and could deliver a dose of 1664 Gy to a 2-cm-diameter, 110- μm -deep region of tissue located 1.5 cm from the window with air between the window and the tissue. This dose level is high enough to consider this technology for medical applications in which shallow energy deposition is beneficial. © 2009 by Radiation Research Society

INTRODUCTION

Pyroelectric materials exhibit a nonzero spontaneous polarization under equilibrium conditions, and this polarization is a function of the material's temperature (1). When a pyroelectric crystal experiences a change in temperature, the resulting electric field from the change in polarization due to the pyroelectric effect is strong enough to cause electron emission (2) and accelerate these electrons to energies of the order of hundreds of keV. Previous work has shown that this effect is strong enough to create compact sources of X rays (3–5),

electrons (6–8), ions (9, 10) and neutrons (via D-D fusion) (11–14). In this paper, we discuss the feasibility of using a pyroelectric accelerator to produce an electron beam for cancer treatment. Low-energy electrons can be used in skin cancer treatment because of their favorable energy deposition relative to depth (15), and there are reports in the literature discussing their utility for a variety of medical and biological applications (16–19).

The pyroelectric materials used in the experiments discussed herein were cylindrical lithium tantalate crystals, with the cylinder's axis parallel to the axis of polarization. At any temperature below the Curie temperature [685°C for LiTaO_3 (20)], the spontaneous polarization of the Z^- face is negative, and the spontaneous polarization of the Z^+ face is positive; the magnitude of this polarization is a function of temperature (1). The pyroelectric effect causes the polarization to decrease during the heating of the crystal. If one were to heat the crystal while it was exposed to the atmosphere, free charges would accumulate on the crystal's surface so as to mask the change in polarization. In a vacuum, however, few free charges are available, and heating the crystal will result in an uncompensated positive charge on the Z^- surface (and an uncompensated negative charge on the Z^+ surface). The reverse effect occurs during cooling. The magnitude of this charge is given by Eq. (1):

$$Q = A\gamma \Delta T, \quad (1)$$

where Q is the surface charge, A is the surface area, γ is the pyroelectric coefficient [176 $\mu\text{C}/\text{m}^2 \text{K}$ for LiTaO_3 (1)] and ΔT is the change in temperature. The increase in charge during the cooling phase creates an electric field. As the electric field strengthens, electron emission occurs at the Z^- surface during cooling (2). Previous work has shown that the electrons emitted from a pyroelectric crystal are nearly monoenergetic (7, 8).

Previous work (8, 12, 21) with pyroelectric accelerators found that in some instances spontaneous discharges of the crystal can occur. These discharges typically take the form of a spark between the crystal surface and ground; if this were to occur in a medical device, it could

¹ Address for correspondence: Rensselaer Polytechnic Institute, Department of Mechanical, Aerospace and Nuclear Engineering, Troy, NY 12180; e-mail: danony@rpi.edu.

result in inconsistent dose rates. However, in the system reported herein, spontaneous discharges did not occur. We attribute this to our use of a relatively large separation distance between the crystal surface and the chamber walls and the window (which are grounded) and to the fact that the crystal was heated at a relatively slow rate (21).

EXPERIMENTAL METHODS

The LiTaO₃ pyroelectric crystals were epoxied to a resistor for heating. The crystal's unexposed (Z⁺) surface was attached to an aluminum block, which was in direct contact with the stainless steel vacuum chamber wall; therefore, the Z⁺ surface was grounded. To allow temperature data to be gathered, a thermocouple was epoxied to the base of the heating resistor. The crystal axis was perpendicular to a 1-cm-diameter × 25-μm-thick beryllium window in the chamber wall. A nickel mesh with 87% electron transmission was used to protect the window from electrical shock due to spontaneous discharge and was flush with the interior of the chamber wall. The electric potential between the exposed face of the crystal and the target (in this case the nickel mesh) can be estimated by modeling the crystal and the gap between the crystal and the target as two capacitors in parallel (12) as in Eq. (2):

$$V = \frac{Q}{C_{\text{sys}}} = \frac{\gamma \Delta T}{\epsilon_0 \left(\frac{\epsilon_{cr}}{d_{cr}} + \frac{1}{d_{gap}} \right)} \approx \frac{\gamma \Delta T}{\frac{\epsilon_0 \epsilon_{cr}}{d_{cr}}}, \quad (2)$$

where ϵ_{cr} is the relative permittivity of the crystal [46 for LiTaO₃ (22)], ϵ_0 is the permittivity of free space, d_{cr} is the thickness of the crystal, and d_{gap} is the distance between the exposed crystal surface and the nickel mesh. Equation (2) typically provides an overestimate of the accelerating potential (23) since it applies to an idealized model. Equation (2) also predicts a linear relationship between crystal thickness and potential; however, experiments have indicated that using crystal thicknesses greater than 1.0 cm is not advantageous (4).

Also of note is the fact that the electron beams emitted by pyroelectric crystals have been shown to be focused within the vacuum chamber (6, 21, 24). When this effect is observed, the beam diameter relative to the distance from the crystal surface is measured and a focal point is determined. In the present arrangement, the focal length was measured to be 0.6 cm (which is inside the vacuum chamber); therefore, the electron beam will diverge as it moves towards the beryllium window. The beam is collimated by the grounded stainless steel flange that supports the beryllium window. The defocusing helps ensure that a more uniform beam arrives at the target.

A LabVIEW program collected electron yield data from the Faraday cup and temperature data from the thermocouple. The Faraday cup was mostly shielded using copper foil, but part of the shield was constructed using thin aluminum foil to allow maximum transmission of X rays to an Amptek CR-100T-CdTe X-ray detector immediately adjacent to the cup. The end point of the measured Bremsstrahlung X-ray spectrum from the Faraday cup was used to estimate the maximum electron energy. The experimental setup is shown in Fig. 1.

Experiments were conducted with three different sizes of crystals. The geometric configurations and the resulting electron yields are summarized in Table 1. The pressure inside the vacuum chamber during these experiments was typically 10⁻⁵ to 10⁻⁴ mbar. The 1-cm-thick × 2-cm-diameter crystal emitted 1.01 × 10¹³ electrons, which is ~14 times the current of the 1-cm-thick × 0.5-cm-diameter crystal. The higher emission from the 2-cm-diameter crystal was expected, since the emitted charge is directly related to the surface area (16 times that of the 0.5-cm-diameter crystal). Using Eq. (1), assuming $\Delta T =$

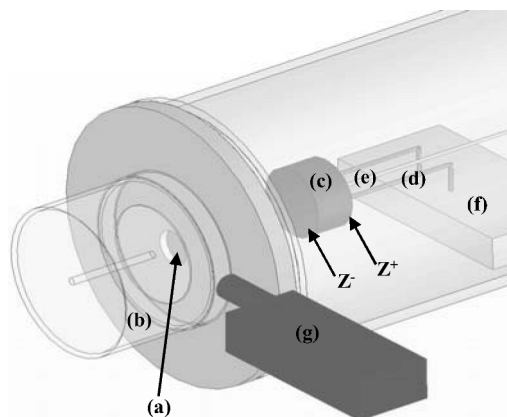


FIG. 1. Drawing of the experimental apparatus used to measure pyroelectric electron emission current and energy. (a) beryllium window, (b) Faraday cup, (c) pyroelectric crystal, (d) heating resistor leads, (e) thermocouple, (f) aluminum base, (g) X-ray detector.

140°C, we calculate the total available charge for the 2-cm-diameter crystal to be 7.7 μC (4.8 × 10¹³ electrons) as opposed to 0.48 μC (3 × 10¹² electrons) for the 0.5-cm-diameter crystals. It was expected that the total emitted charge for the 1-cm-thick × 0.5-cm-diameter crystal and the 4-cm-thick × 0.5-cm-diameter crystal would be about the same, since their Z⁻ surfaces have the same area. However, due to the low thermal conductivity of LiTaO₃ [~4 W/m K (25)], the 4-cm-thick crystal did not achieve as high a temperature as the 1-cm-thick crystal; consequently, fewer emitted electrons were observed when using the 4-cm-thick crystal.

The observed temperature and electron current for the 1-cm-thick × 0.5-cm-diameter crystal are plotted as a function of time (10) in Fig. 2. As shown in this plot, the back face of the crystal experiences a ΔT of ~140°C. The apparent delay in electron emission relative to the end of the heating phase is due to the low thermal conductivity of the crystal, and the fact that the temperature was measured at the end of the crystal opposite from the electron-emitting surface. During the cooling of the crystal, X-ray spectra were gathered at 3-min intervals and the respective end point energies as a function of time are shown in Fig. 3. The maximum X-ray energy, which is indicative of the electron energy, was observed to be 125 keV. As can be seen in Fig. 3, the electron emission energy remained constant for approximately 8 min, during which time a constant dose rate and penetration depth are provided. This maximum energy plateau was preceded and succeeded by a transition from and to lower energies.

DOSE CALCULATIONS

A pyroelectric crystal system can be engineered to individual tissue penetration requirements by varying

TABLE 1
Electron Emission from Various Experimental Configurations

Crystal thickness	Diameter	Distance to nickel mesh	Measured electrons	Calculated electrons
1 cm	2 cm	0.5 cm	1.01 × 10 ¹³	4.8 × 10 ¹³
4 cm	0.5 cm	1 cm	1.85 × 10 ¹¹	3.0 × 10 ¹²
1 cm	0.5 cm	1.5 cm	6.98 × 10 ¹¹	3.0 × 10 ¹²

Note. Also shown are the calculated electron yield and potential determined using Eqs. (1) and (2), respectively, for $\Delta T = 140^\circ\text{C}$.

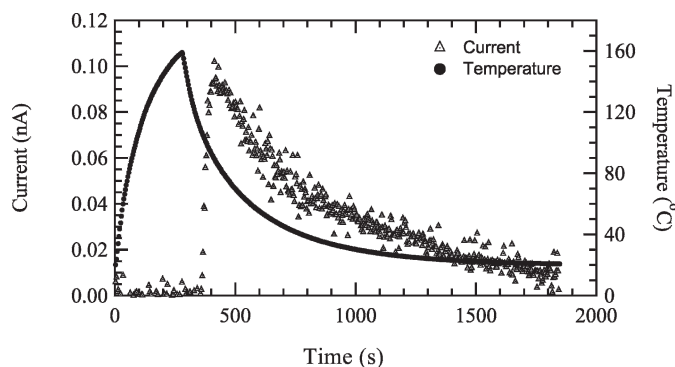


FIG. 2. Current and temperature as a function of time for a 1-cm \times 0.5-cm lithium tantalate crystal. Temperature was measured at the grounded surface of the crystal; the temperature at the exposed surface of the crystal would be lower.

the maximum accelerating energy of the crystal by using different crystal sizes and temperature profiles; a smaller ΔT would result in a lower accelerating potential and therefore lower electron energies. The diameter of the electron beam can also be customized by varying the geometry of the system. To characterize LiTaO₃ crystals for medical applications, dose calculations were performed using data from the cooling phase of the 1-cm-thick \times 2-cm-diameter crystal (1.01×10^{13} electrons with an energy of 100 keV). It was assumed that the crystal emitted a monoenergetic beam of electrons with a diameter of 1 cm. We define our treatment volume as a 2-cm-diameter, 110- μ m-thick region of soft tissue.

The behavior of the electrons was evaluated using an MCNP Monte Carlo simulation (26). In the MCNP simulation, the electron source was taken to be a 1-cm-diameter monoenergetic electron source perpendicular to a 25- μ m-thick, 1-cm-diameter beryllium window that was located in a 1-cm-thick steel wall. The electrons then traveled through 0.5 cm of air before crossing the plane of the outer surface of the steel wall and then traveled through an additional 1 cm of air before reaching the surface of a region of soft tissue. The geometry used in MCNP is shown in Fig. 4. After passing through 25 μ m of beryllium and 1.5 cm of air, the energy of the electrons will be reduced. The energy spectrum of the electrons incident upon the surface of the tissue was calculated using MCNP and is shown in Fig. 5; the peak energy is 80 keV. Furthermore, it was found that due to scattering in the 1 cm of air, only 84% of the electrons measured by the Faraday cup would strike within the treatment area, with the remainder striking outside this area. A plot of the radial distribution of electrons is given in Fig. 6.

The MCNP simulations were used to evaluate the dose delivered to the treatment volume (27). To accomplish this, the geometry of the tissue was modeled as follows in MCNP: A 2-cm-diameter cylinder of tissue with a depth of 200 μ m is coaxial with the electron source and beryllium window and was divided into 10-

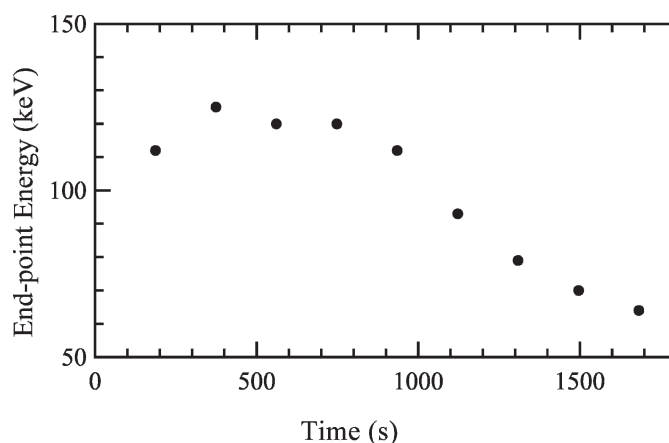


FIG. 3. Electron energy measured from the end point of the X-ray spectrum resulting from interactions of the electrons with the copper Faraday cup for the 1-cm \times 0.5-cm lithium tantalate crystal. For this arrangement, Eq. (2) predicts a potential of 596 kV (assuming $\Delta T = 140^\circ\text{C}$).

μ m-thick slices, the first 11 of which form the treatment volume. This cylinder of tissue is surrounded by a doughnut of tissue to account for scattering to and from the surrounding tissue and to quantify energy deposition to the surrounding tissue. The energy deposited in each of these 21 cells and the surrounding tissue is determined using the *8 tally in MCNP. The total dose delivered to

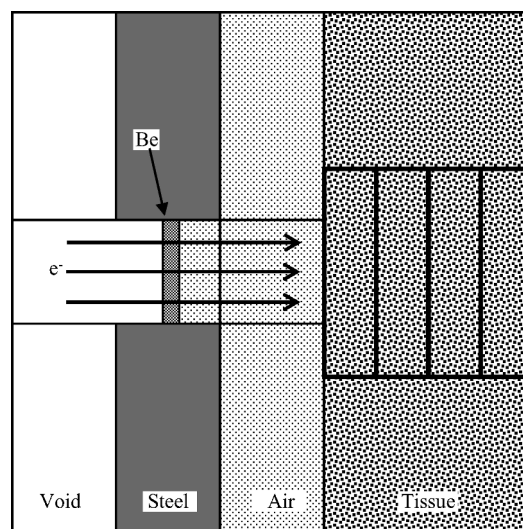


FIG. 4. MCNP geometry (not to scale). Electrons are emitted from a monoenergetic (100 keV) disk source with a diameter of 1 cm located in a void. Electrons travel through a 25- μ m-thick beryllium window before entering a 1.5-cm-thick region of air before impinging on a region of soft tissue. This region is modeled as a 2-cm-diameter cylinder of tissue with a depth of 200 μ m divided into 10- μ m-thick slices, the first 11 of which form the treatment volume (for clarity, only four slices are shown in the figure). This cylinder of tissue is surrounded by a doughnut of tissue to account for scattering to and from the surrounding tissue and to quantify energy deposition to the surrounding tissue.

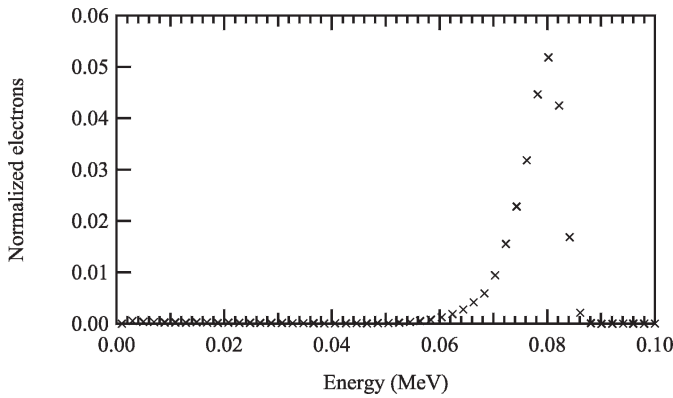


FIG. 5. Energy spectrum of the electrons incident upon the surface of the skin calculated using MCNP. Values are normalized for one source electron.

the treatment volume is calculated using Eq. (3):

$$\text{Total Dose} = \frac{N_e \sum_{i=0}^{N-1} \Delta E_i}{\rho A \sum_{i=0}^{N-1} x}, \quad (3)$$

where N_e is the number of electrons incident upon the treatment area, ρ is the density of the material (1.0 g/cm^3 for tissue), A is the area to be treated (1.0-cm -radius circle), x is the thickness of each layer, ΔE_i is the energy deposited in the i th layer, and N is the number of layers, in this case 11, in the treatment volume. The total dose to the treatment volume was 1664 Gy; a few electrons penetrated deeper, and the nine layers below the treatment volume received a total dose of 1.3 Gy. The dose to each of the individual $10\text{-}\mu\text{m}$ -thick layers in the treatment volume was calculated by dividing the energy deposited in each layer by its mass; the results are plotted in Fig. 7. Some electrons scattered out of the treatment volume and into the surrounding tissue and some of the electrons struck the skin outside of the treatment area; as a result, the surrounding tissue absorbed 15% of the total energy absorbed by all of the tissue. A dose calculation for the surrounding tissue is not meaningful due to its large (and arbitrary) volume.

A simple calculation of the dose was also performed. Values for the range and stopping power of electrons in soft tissue were obtained from ESTAR (28). It was found that 80 keV electrons would penetrate a distance of $97 \mu\text{m}$. The treatment volume was defined as a 2-cm -diameter cylinder with a depth of $107 \mu\text{m}$ (ESTAR depth + 10%). Assuming that all of the energy from the (monoenergetic) electrons was absorbed by the treatment volume, the dose was 3251 Gy. This value is higher than what was calculated by MCNP; however, the simple calculation does not account for scattering and the fact that a some of the incident energy is delivered to the surrounding tissue. Furthermore, the simple calculation assumed that all of the electrons had an energy of

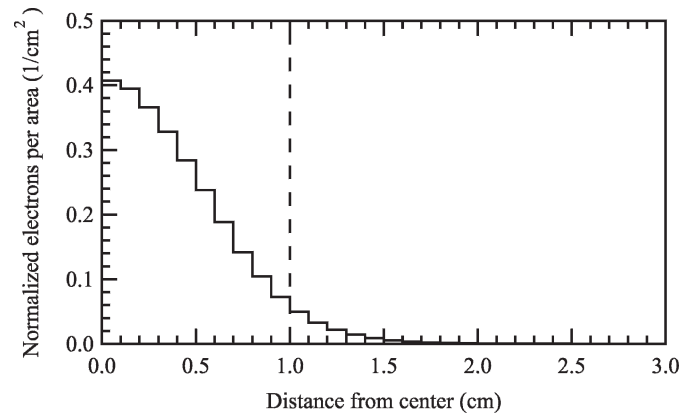


FIG. 6. Radial distribution of the electron flux incident upon the surface of the skin calculated using MCNP. Values are normalized for one source electron. The dashed line indicated the boundary of the treatment volume.

80 keV when they reached the surface of the skin; we know from Fig. 5 that many of the electrons were of lower energy. The reasonableness of this explanation of the discrepancy can be assessed by examining the total energy deposited (rather than dose) in the tissue. According to the simple calculation, 109 mJ of energy was absorbed by the treatment volume, whereas the MCNP calculations indicate that 58 mJ was absorbed by the treatment volume and 9.8 mJ was absorbed by the surrounding tissue.

CONCLUSION

The pyroelectric electron emission experiments showed that an inexpensive source of electrons delivered to air could be developed using pyroelectric crystals and that such a source could deliver a large dose over a thin penetration depth in tissue. This type of electron source can have potential applications when shallow dose is required. Multiple applications of small quantities of doses can result in a dose sufficient for treatment. Smaller doses can be attained by using crystals with a smaller surface area or by using a smaller temperature

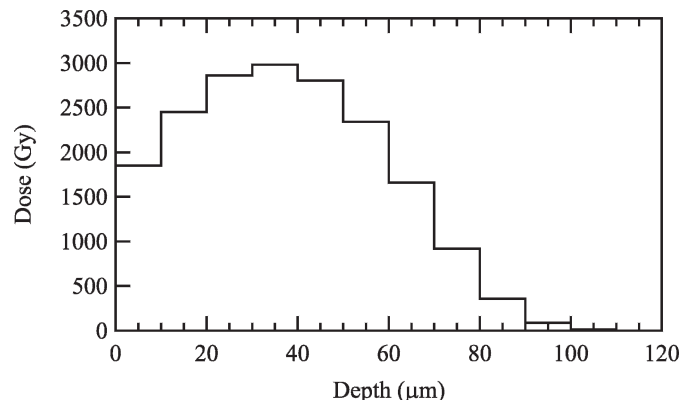


FIG. 7. Dose as a function of depth as delivered to $10\text{-}\mu\text{m}$ -thick slices calculated using MCNP with 3.77×10^{12} incident electrons.

change. We envision that this technology can be used to build a portable, battery-operated electron irradiation device.

ACKNOWLEDGMENT

This work was supported by the U.S. Department of Energy under DOE NEER grant number 04ID14596.

Received: May 29, 2009; accepted: June 22, 2009

REFERENCES

1. S. B. Lang, Pyroelectricity: From ancient curiosity to modern imaging tool. *Phys. Today* **58**, 31–36 (2005).
2. G. Rosenman, D. Shur, Ya. E. Krasik and A. Dunaevsky, Electron emission from ferroelectrics. *J. Appl. Phys.* **88**, 6109–6161 (2000).
3. J. D. Brownridge, Pyroelectric X-ray generator. *Nature* **358**, 287–288 (1992).
4. J. A. Geuther and Y. Danon, High-energy x-ray production with pyroelectric crystals. *J. Appl. Phys.* **97**, 104916 (2005).
5. J. D. Brownridge and S. Raboy, Investigations of pyroelectric generation of x rays. *J. Appl. Phys.* **86**, 640–647 (1999).
6. J. D. Brownridge and S. M. Shafroth, Self-focused electron beams produced by pyroelectric crystals on heating or cooling in dilute gases. *Appl. Phys. Lett.* **79**, 3364–3366 (2001).
7. J. D. Brownridge, S. M. Shafroth, D. W. Trott, B. R. Stoner and W. M. Hooke, Observation of multiple nearly monoenergetic electron production by heated pyroelectric crystals in ambient gas. *Appl. Phys. Lett.* **78**, 1158–1159 (2001).
8. J. A. Geuther and Y. Danon, Electron and positive ion acceleration with pyroelectric crystals. *J. Appl. Phys.* **97**, 074109 (2005).
9. E. L. Neidholdt and J. L. Beauchamp, Compact ambient pressure pyroelectric ion source for mass spectrometry. *Anal. Chem.* **79**, 3945–3948 (2007).
10. J. A. Geuther and Y. Danon, Applications of pyroelectric particle accelerators. *Nucl. Instrum. Methods B* **261**, 110–113 (2007).
11. B. Naranjo, J. K. Gimzewski and S. Putterman, Observation of nuclear fusion driven by a pyroelectric crystal. *Nature* **434**, 1115–1117 (2005).
12. J. A. Geuther, Y. Danon and F. Saglime, Nuclear reactions induced by a pyroelectric accelerator. *Phys. Rev. Lett.* **96**, 054803 (2006).
13. D. Gillich, A. Kovanen, B. Herman, T. Fullem and Y. Danon, Pyroelectric crystal neutron production in a portable prototype vacuum system. *Nucl. Instrum. Methods A* **602**, 306–310 (2009).
14. D. J. Gillich, R. Teki, T. Z. Fullem, A. Kovanen, E. Blain, D. B. Chrisey, T.-M. Lu and Y. Danon, Enhanced pyroelectric crystal D-D nuclear fusion using tungsten nanorods. *Nano Today* **4** 227–234 (2009).
15. J. A. O'Donoghue and T. E. Wheldon, Targeted radiotherapy using Auger electron emitters. *Phys. Med. Biol.* **41**, 1973–1992 (1996).
16. W. E. Wilson, D. J. Lynch, K. Wei and L. A. Braby, Microdosimetry of a 25 keV electron microbeam. *Radiat. Res.* **155**, 89–94 (2001).
17. M. S. Resat and W. F. Morgan, Microbeam developments and applications: A low linear energy transfer perspective. *Cancer Metastasis Rev.* **23**, 323–331 (2004).
18. E. H. Kim, G. M. Sun and M. Jang, An electron microbeam cell-irradiation system at KIRAMS: Performance and preliminary experiments. *Radiat. Prot. Dosimetry* **122**, 297–300 (2006).
19. D. E. Bordelon, J. Zhang, S. Graboski, A. Cox, E. Schreiber, O. Z. Zhou and S. Chang, A nanotube based electron microbeam cellular irradiator for radiobiology research. *Rev. Sci. Instrum.* **79**, 125108 (2008).
20. S. Kim, V. Gopalan, K. Kitamura and Y. Furukawa, Domain reversal and nonstoichiometry in lithium tantalate. *J. Appl. Phys.* **90**, 2949–2963 (2001).
21. J. D. Brownridge and S. M. Shafroth, Using static charge on pyroelectric crystals to produce self-focusing electron and ion beams and transport through tubes. *J. Electrostat.* **63**, 249–259 (2005).
22. R. T. Smith, Elastic, piezoelectric, and dielectric properties of lithium tantalate. *Appl. Phys. Lett.* **11**, 146–148 (1967).
23. A. Kovanen, Y. Danon and D. Gillich, X-ray production using stacked pyroelectric crystals. *ANS Trans.* **98**, 406–407 (2008).
24. N. Kukhtarev, J. D. T. Kukhtareva, M. Bayssie, J. Wang and J. D. Brownridge, Generation of focused electron beam by pyroelectric and photogalvanic crystals. *J. Appl. Phys.* **96**, 6794–6798 (2004).
25. S. Longuemart, A. H. Sahraoui, D. Dadarlat, S. Delenclos, C. Kolinsky and J. M. Buisins, Study of thermal parameter temperature dependence of pyroelectric materials. *Rev. Sci. Instrum.* **74**, 805–807 (2003).
26. R. A. Forster, L. J. Cox, R. F. Barrett, T. E. Booth, J. F. Briesmeister, F. B. Brown, J. S. Bull, G. C. Geisler, J. T. Goorley and A. Sood, MCNP™ Version 5. *Nucl. Instrum. Methods B* **213**, 82–86 (2004).
27. N. Reynaert, H. Palmans, H. Thierens and R. Jeraj, Parameter dependence of the MCNP electron transport in determining dose distributions. *Med. Phys.* **29**, 2446–2454 (2002).
28. M. J. Berger, J. S. Coursey, M. A. Zucker and J. Chang, ESTAR v. 1.2.3. National Institute of Standards and Technology, Gaithersburg, MD, 2005. [Available online at <http://physics.nist.gov/Star>]